Thermally driven isosymmetric phase transitions and structure–bioactivity relationships in a hybrid tetrachlorocuprate(II)

Sandra Walha[a,b], Rageh K. Hussein[c], Imen Rekik[d,e], Mokhtar Hjiri[c], Ali Ben Ahmed[f,g*], Houcine Naïli[a], Thierry Bataille[h]

[a]*Laboratoire Physico-Chimie de l'Etat Solide, Département de Chimie, Faculté des Sciences de Sfax, BP1171, 3000 Sfax, Tunisia.*
[b]*Department of chemical, Preparatory Institute for Engineering Studies of Gabes, Gabes 6029, Tunisia.*
[c]*Physics Department, College of Science, Imam Mohammad Ibn Saud Islamic University (IMSIU), Riyadh 11623, Saudi Arabia*
[d]*University of Sfax, Centre of Biotechnology of Sfax, Laboratory of Microbial and Enzymatic Biotechnologies and Biomolecules, Road of Sidi Mansour Km 6, P.O. Box 1177, Sfax 3018, Tunisia.*
[e]*University of Gabes, Faculty of Sciences of Gabes, Department of biology, Gabes 6029, Tunisia.*
[f]*University of Sfax, Higher Institute of Biotechnology of Sfax, Department of Biomedical, BP 1175 - 3000 Sfax, Tunisia.*
[g]*University of Sfax, Faculty of Sciences of Sfax, Department of Physics, Laboratory of Applied Physics, BP 1171, 3000, Sfax, Tunisia.*
[h]*Ecole Nationale Supérieure de Chimie de Rennes, CNRS, ISCR (Institut des Sciences Chimiques de Rennes) - UMR 6226, F-35000 Rennes, France.*

***Corresponding authors:** ali.benahlmed@isbs.usf.tn ; https://orcid.org/0000-0001-8560-2630

1.1. Synthesis of $(C_5H_9N_3)CuCl_4$

Plate-like crystals of the studied compound were obtained at room temperature by slow evaporation of an aqueous solution prepared from 2,5-diaminopyridine dihydrochloride ($C_5H_7N_3 \cdot 2HCl$), copper(II) chloride dihydrate ($CuCl_2 \cdot 2H_2O$), and concentrated hydrochloric acid, mixed in a 1:2:1 molar ratio. The reactants were dissolved in distilled water under continuous magnetic stirring at 600 rpm for 30 min, during which the pH of the reaction mixture was adjusted to approximately 1.5 by the addition of concentrated HCl. The resulting clear solution was then filtered and allowed to stand undisturbed at room temperature for 10–12 days, leading to the formation of well-defined plate-like crystals via evaporation. After completion of crystallization, the crystals were collected by filtration, rinsed with a small amount of cold distilled water, and dried in air. Elemental microanalysis for $(C_5H_9N_3)CuCl_4$: calcd (%) C, 18.66; H, 2.23; N, 13.03; found (%) C, 18.95; H, 2.38; N, 13.26. The reaction yield was 0.498 g (97%). ESI-MS (negative mode) m/z: $[M - H]^-$ calcd 316.47, found 316.29.

1.2. Powder X-Ray diffraction

Temperature-dependent X-ray diffraction (TD-XRD) measurements were performed using a D5005 powder diffractometer (Bruker AXS) equipped with Cu Kα radiation [λ(Kα1) = 1.5406 Å, λ(Kα2) = 1.5444 Å], selected by a diffracted-beam graphite monochromator. The instrument was fitted with an Anton Paar HTK1200 high-temperature oven camera. Diffraction patterns were collected over the temperature range room temperature to 700 °C, with a heating rate of 5 °C min^{-1}. At each selected temperature, the sample was held for an equilibration time of 10 min prior to data acquisition to ensure thermal stability.

1.3. Single crystal X-Ray diffraction

Single-crystal X-ray diffraction (SCXRD) data were collected on a Siemens APEX II four-circle diffractometer equipped with monochromatic Mo Kα radiation (λ = 0.71073 Å). Well-formed, small single-domain crystals were carefully chosen for analysis, and measurements were carried out at four different temperatures: 293, 343, 368, and 393 K, in order to investigate possible structural variations with thermal effects. Absorption corrections were applied using the multi-scan procedure implemented in the program SADABS [1], which relies on multiple and symmetry-equivalent reflections to minimize systematic errors. The determination of the crystal structure followed the automated space group search incorporated in the WINGX [2]. The positions of the heavier atoms (Cu and Cl) were successfully obtained using direct methods with SHELXS-97 [3]. Fourier difference maps enabled the localization of the remaining non-hydrogen atoms of the organic moiety, refined with the program SHELXL-97 [4]. Hydrogen atoms attached to carbon and nitrogen were placed at idealized geometrical positions and refined using the riding model, with fixed bond distances of C–H = 0.93 Å and N–H = 0.89 Å, in accordance with standard refinement protocols.

1.4. Spectroscopic measurements

The infrared spectrum was obtained with a PerkinElmer BX FT-IR spectrometer fitted with a DTGS detector, covering the 400–4000 cm^{-1} region at a spectral resolution of 0.8 cm^{-1}. Each spectrum represents the average of 32 accumulated scans. Measurement was carried out on solid sample without KBr dilution.

1.5. Thermal and dielectric experiments

The differential scanning calorimetry (DSC) measurements were performed using a SETARAM DSC131 instrument over the temperature range 40–350 °C at a heating rate of 5 °C min^{-1}. A polycrystalline sample weighing 8.08 mg was sealed in a hermetic aluminium

crucible. The DSC experiments were conducted under a flowing air atmosphere to ensure consistency with the thermogravimetric analysis conditions. Thermogravimetric (TGA) and differential thermal analysis (DTA) measurements were carried out using a SETARAM MULTI-MODULE 92 analyzer from room temperature to 500 °C at an average heating rate of 5 °C min^{-1}, under a flowing air atmosphere with a flow rate of 50 mL min^{-1}. Identical atmospheric conditions were applied in both DSC and TGA/DTA experiments to ensure data comparability.

The dielectric permittivity (ε^*) measurements were recorded with an impedance analyzer Hewlett–Packard 4192 ALF in the frequency range from 1–1000 kHz. Crystals of the title compound were crushed and pressed to dense and translucent pellets (12 mm in diameter 0.8 mm in thickness) at a pressure of 200 MPa. Both planar faces of these pellets were coated with silver paint and the pellets were then sandwiched between metal electrodes, which were also coated with silver paint.

1.6. Biologic tests

1.6.1. Antibacterial activity

The antibacterial activity of 2-amino-5-ammoniopyridinium tetrachlorocuprate(II) (1) and its organic precursor 2-amino-5-aminopyridine (2) was evaluated using the agar well diffusion method against selected Gram-positive and Gram-negative bacterial strains [5–7]. Owing to their limited solubility in water, both compounds were initially dissolved in dimethyl sulfoxide (DMSO) to prepare stock solutions at a concentration of 10 mM, which were subsequently diluted with sterile distilled water to obtain working solutions of 25, 50, and 100 µM. The final DMSO concentration in all test solutions was maintained below 1% (v/v) to exclude any solvent-related antibacterial effects. Sterile wells were filled with 100 µL of each test solution, and the inoculated agar plates were incubated at 37 °C for 24 h. The diameters of the inhibition zones were measured in millimeters. All experiments were performed in triplicate, and the results are expressed as mean ± standard deviation (SD). Standard antibiotics were used as positive controls, while DMSO at the same concentration served as a negative control. Statistical significance was evaluated using one-way ANOVA, with $p < 0.05$ considered statistically significant.

1.6.2. Anti-inflammatory activity

The in vitro anti-inflammatory activity of compound (**1**) and its organic precursor (**2**) was assessed using the bovine serum albumin (BSA) protein denaturation assay and the human red blood cell (HRBC)

membrane stabilization method. BSA (fraction V, ≥98% purity) was obtained from a commercial supplier and prepared freshly in distilled water. For the protein denaturation assay, solutions of each compound were prepared at concentrations of 25, 50, 100, and 200 μg·mL^{-1}. To each sample, 0.2 mL of egg albumin, 2.8 mL of phosphate-buffered saline (PBS, pH 6.4), and the test compound were mixed and incubated at 37 ± 1 °C for 15 min, followed by heating at 70 °C for 5 min to induce protein denaturation. After cooling to room temperature, the absorbance was measured at 660 nm using a UV–Vis spectrophotometer. Diclofenac sodium was used as the reference anti-inflammatory drug. The percentage inhibition of protein denaturation was calculated using the following equation:

$$Inhibition\ (\%) = \frac{A_1 - A_0}{A_1} \times 100 \qquad (1)$$

Where A_1 is the absorbance of the control and A_0 is the absorbance of each sample.

1.7. Computational methods

1.7.1. Computational docking analysis

Molecular docking studies were performed using the CBDOCK2 server to evaluate the binding interactions of the copper(II) complex $(C_5H_9N_3)CuCl_4$ with a series of biological targets. The complex was docked against three bacterial proteins, namely IS16 (PDB ID: 1516), IscU Fe–S cluster assembly protein (PDB ID: P3W3), and Catalase (PDB ID: 1SJ2), as well as five anti-inflammatory targets including iNOS (PDB ID: 1NSI), 5-LOX (PDB ID: 3O8Y), COX-2 (PDB ID: 5KIR), xanthine oxidase (PDB ID: 1FIQ), and TNF-α (PDB ID: 2AZ5). Docking calculations were carried out using the AutoDock Vina scoring function, and the resulting binding poses were analyzed and visualized with Discovery Studio software. The interaction profiles were examined in detail to identify key molecular contacts such as conventional hydrogen bonds, hydrophobic interactions, π–π stacking, and π–sigma interactions, providing valuable insight into the potential biological activity and mechanism of action of the studied complex.

1.7.2. Density Functional Theory calculation

Density Functional Theory (DFT) calculations were performed using Gaussian 16 [8]. The ground-state geometries of the investigated compounds were optimized by searching for the minimum on the potential energy surface, ensuring that the total electronic energy reached a stable equilibrium configuration. These quantum-chemical calculations were further employed to support the analysis of the experimental spectroscopic features through simulated vibrational and electronic data. All computations were performed with the wb97xd functional [9] in combination with the Land2z [10] basis set. All calculations were performed within the static electric field (finite-field) approach at the same DFT level as the geometry optimizations,

ensuring methodological consistency. Optimized geometries corresponded to true minima, confirmed by the absence of imaginary frequencies. Molecular visualizations were generated using GaussView interface [11].

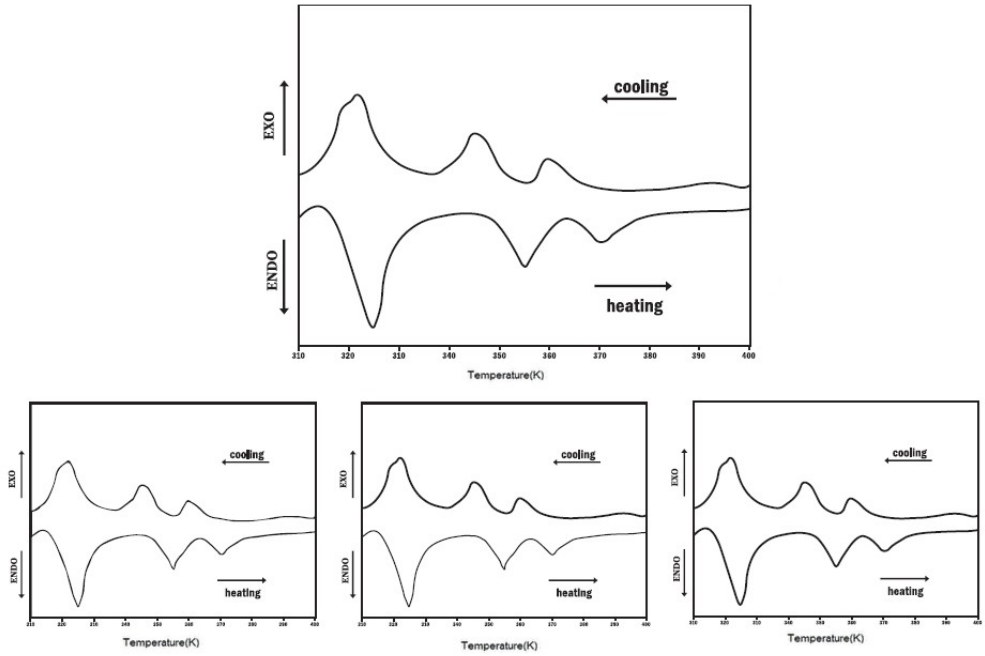

Fig. S1 DSC measurements over multiple consecutive heating–cooling cycles under identical conditions

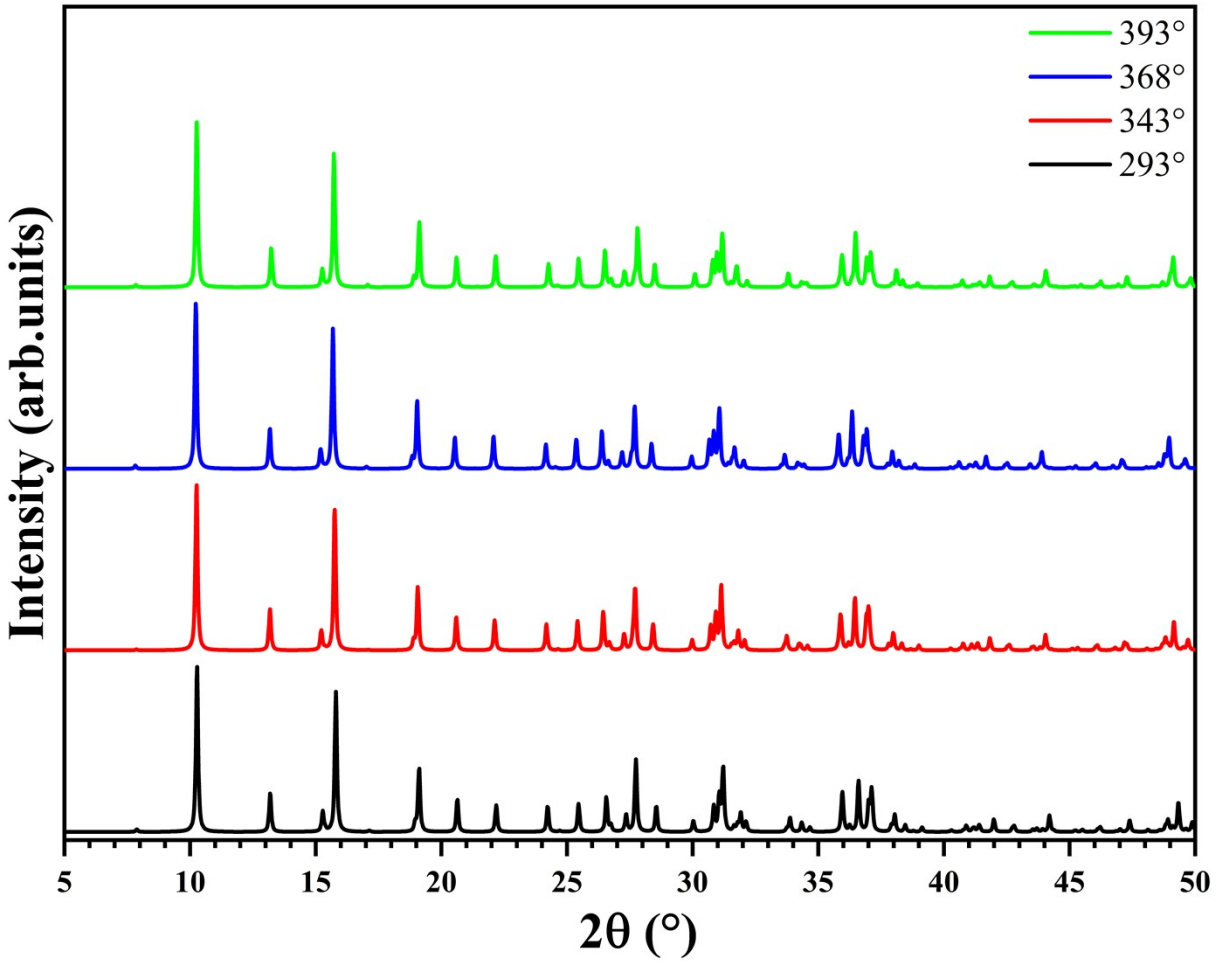

Fig. S2 The simulated powder X-ray diffraction (PXRD) patterns of $(C_5H_9N_3)CuCl_4$

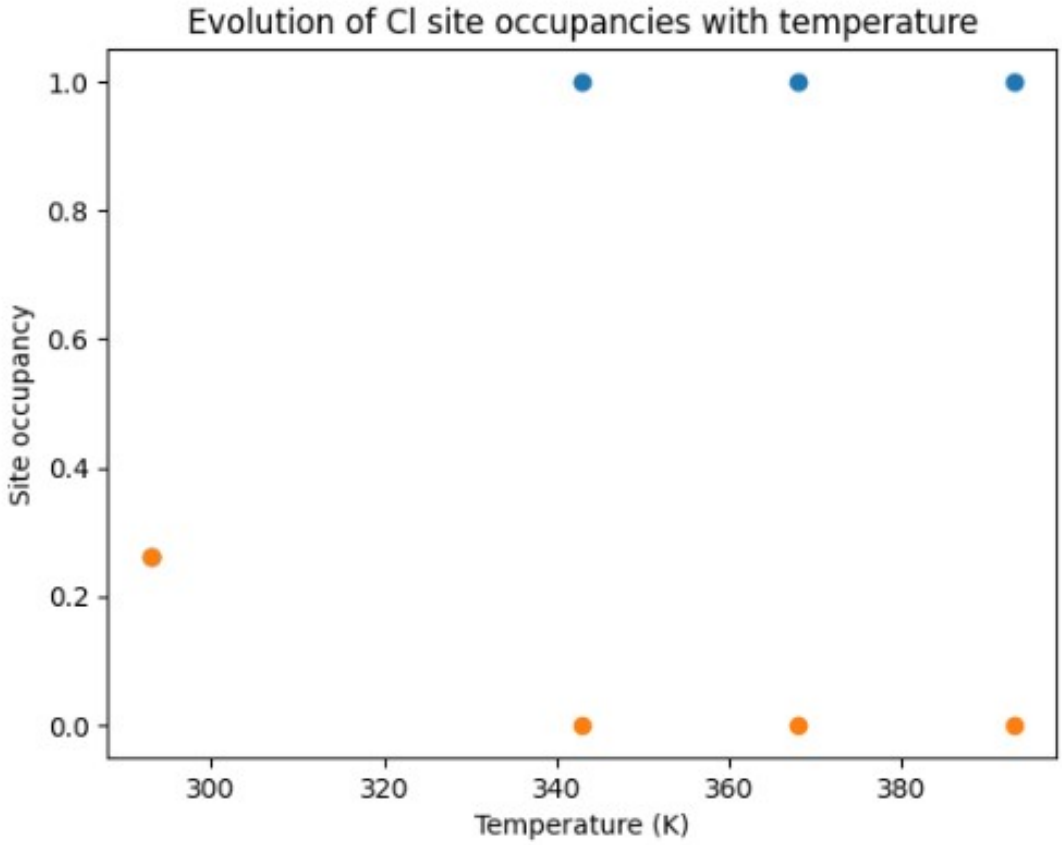

Fig. S3 Evolution of the site occupancies of the disordered chlorine atoms as a function of temperature. Blue and orange symbols correspond to the occupancies of the Cl1A and Cl1B split sites, respectively

Table S1 Selected bond distances (Å) and bond angles (°) for compound $(C_5H_9N_3)CuCl_4$

A T = 293K			
Square- pyramidal around Cu		Within the organic moiety	
Cu1—Cl1	2.273 (2)	N1—C1	1.317 (6)
Cu1—Cl1^{i}	2.273 (2)	N2—C1	1.362 (6)
Cu1—Cl1^{ii}	2.492 (3)	N2—C5	1.372 (6)
Cu1—Cl2	2.253 (2)	N3—C4	1.459 (6)
Cu1—Cl2^{i}	2.253 (2)	C4—C5	1.356 (6)
Cu1—Cl3	2.845 (15)	C3—C4	1.385 (6)
Cl1—Cu1^{iii}	2.492 (3)	C1—C2	1.385 (6)
Cl2^{i}—Cu1—Cl2	88.4 3 (7)	C2—C3	1.362 (7)
Cl2^{i}—Cu1—Cl1	169.55 (7)	C1—N2—C5	121.3 (4)
Cl2—Cu1—Cl1	98.18 (7)	N1—C1—N2	120.3 (4)
Cl1—Cu1—Cl1^{i}	74.19 (2)	N1—C1—C2	121.4 (4)
Cl2—Cu1—Cl1^{ii}	170.90 (6)	N2—C1—C2	118.3 (4)
Cl1—Cu1—Cl1^{ii}	90.74 (5)	C3—C2—C1	120.6 (4)
Cl2—Cu1—Cl3	91.61 (4)	C2—C3—C4	120.0 (4)
Cl1—Cu1—Cl3	96.22 (5)	C5—C4—C3	119.4 (4)
Cl1^{ii}—Cu1—Cl3	85.53 (5)	C5—C4—N3	120.6 (4)
Cu1—Cl1—Cu^{iii}	107.59 (7)	C3—C4—N3	120.0 (4)
Cl2^{i}—Cu1—Cl1^{ii}	83.01 (6)	C4—C5—N2	120.4 (4)
A T = 343K			
Square- pyramidal around Cu		Within the organic moiety	
Cu1—Cl1	2. 359 (2)	C1—N1	1.319 (8)
Cu1—Cl1^{i}	2.359 (2)	N2—C4	1.456 (7)
Cu1—Cl2	2.262 (14)	N3—C1	1.360 (7)
Cu1—Cl2^{i}	2.262 (14)	N3—C5	1.360 (8)
Cl1—Cu1^{ii}	2.359 (11)	C1—C2	1.398 (7)
Cu1—Cl3	2. 849 (19)	C2—C3	1.357 (8)
Cl2^{i}—Cu1—Cl2	88.39 (8)	C3—C4	1.401 (7)
Cl2^{i}—Cu1—Cl1^{i}	177.17 (6)	C4—C5	1.363 (8)
Cl2—Cu1—Cl1^{i}	90.20 (5)	N1—C1—C2	121.6 (5)
Cl2^{i}—Cu1—Cl1^{i}	90.20 (5)	N1—C1—N3	121.2 (5)
Cl2—Cu1—Cl1	177.17 (6)	N2—C4—C3	119.2 (5)
Cl1^{i}—Cu1—Cl1	91.10 (5)	N3—C5—C4	119.7 (5)
Cl2^{i}—Cu1—Cl3	91.85 (5)	C5—N3—C1	122.8 (5)
Cl2—Cu1—Cl3	90.65 (4)	C1—C2—C3	121.4 (5)
Cl1—Cu1—Cl3	90.65 (4)	C2—C3—C4	119.3 (5)
Cu1—Cl1—Cu^{ii}	110.04 (7)	C3—C4—C5	119.6 (5)
A T = 368K			
Square- pyramidal around Cu		Within the organic moiety	
Cu1—Cl1	2.357 (4)	C5—C6	1.373 (9)
Cu1—Cl1^{i}	2.357 (4)	C6—N2	1.411 (9)
Cu1—Cl3	2.274 (8)	N3—C4	1.327 (9)
Cu1—Cl3^{i}	2.274(8)	N2—C8	1.360 (9)
Cu1—Cl2	2.861 (2)	C4—C8	1.383 (9)
Cl1—Cu1^{ii}	2. 357 (13)	C3—C4	1.379 (9)
Cl1—Cu1—Cl2	90.91 (4)	C5—C3	1.343 (9)
Cl1^{i}—Cu1—Cl2	90.91 (4)	C6—N2—C8	119.1 (6)
Cl2—Cu1—Cl3	92.00 (6)	N3—C4—C3	120.9 (6)
Cl1—Cu1—Cl1^{i}	91.40 (6)	N3—C4—C8	121.5 (6)
Cl3—Cu1—Cl1	90.36 (7)	N2—C6—N1	119.6 (4)
Cl3^{i}—Cu1—Cl1	176.58 (7)	N2—C8—C4	121.6 (4)
Cl3^{i}—Cu1—Cl3	87.73 (2)	N2—C5—C6	119.0 (6)
Cl1^{i}—Cu1—Cl3^{i}	90.36 (6)	C3—C5—C6	120.3 (6)
Cl2—Cu1—Cl3^{i}	92.00 (6)	C4—C3—C5	122.3 (5)
Cu1—Cl1—Cu^{ii}	110.35 (9)	C3—C4—C8	117.6 (6)
Cl1^{i}—Cu1—Cl 3	176.58 (7)	C3—C4—C5	120.4 (4)
A T = 393K			
Square- pyramidal around Cu		Within the organic moiety	
Cu1—Cl1	2. 341 (2)	C1—N3	1.463 (10)
Cu1—Cl1^{i}	2.341 (2)	N2—C1	1.404 (10)
Cu1—Cl2	2.267 (2)	N1—C3	1.303 (11)
Cu1—Cl2^{i}	2.267 (15)	N2—C2	1.334 (12)
Cl1—Cu1^{ii}	2.341 (15)	C1—C5	1.356 (11)
Cu1—Cl3	2. 873 (3)	C2—C3	1.415 (11)
Cl2^{i}—Cu1—Cl2	86.78 (7)	C3—C4	1.379 (11)
Cl2^{i}—Cu1—Cl1^{i}	176.05 (9)	C4—C5	1.357 (11)
Cl2—Cu1—Cl1^{i}	90.69 (9)	N1—C3—C2	123.0 (8)
Cl2^{i}—Cu1—Cl1	90.69 (9)	N2—C2—C3	122.4 (7)
Cl2—Cu1—Cl1	176.05 (6)	N2—C1—N3	119.5 (7)

Cl1^{i}—Cu1—Cl1	91.67 (6)	C5—C1—N2	120.1 (8)
Cl2^{i}—Cu1—Cl3	91.93 (7)	C5—C1—N3	120.5 (7)
Cl2—Cu1—Cl3	91.93 (7)	C4—C5—C1	119.2 (7)
Cl1^{i}—Cu1—Cl3	91.19 (5)	C5—C4—C3	123.5 (7)
Cu1—Cl1—Cu^{ii}	110.41 (5)	C4—C3—C2	115.3 (7)
Cl1—Cu1—Cl3	91.19 (5)	C4—C3—N1	121.7 (8)
Symmetry codes: At 293 K: (i) −*x*+1, *y*, *z*; (ii) *x*+1/2, *y*, −*z*+1/2; (iii) *x*−1/2, *y*, −*z*+1/2; At 343 K: (i) –x+1, y, z; (ii) −x+1/2, y, −z+1/2; At 368: (i) −x, y, z; (ii) −x+1/2, y, -z+1/2; At 393: (i) –x+1, y, z; (ii) −x+1/2, y, −z+1/2.			

Table S2 Comparison of selected Cu–Cl bond lengths (Å) and Cl–Cu–Cl bond angles (°) at 343 K and 368 K

Parameter	343 K	368 K
Cu–Cl bond lengths (Å)		
Cu1–Cl1	2.359(2)	2.357(4)
Cu1–Cl1^{i}	2.359(2)	2.357(4)
Cu1–Cl2	2.262(14)	2.274(8)
Cu1–Cl2^{i}	2.262(14)	2.274(8)
Cu1–Cl3 (axial)	2.849(19)	2.861(2)
Cl–Cu–Cl bond angles (°)		
Cl1–Cu1–Cl1^{i}	88.39(8)	90.91(4)
Cl2–Cu1–Cl2^{i}	90.20(5)	90.91(4)
Cl1–Cu1–Cl2	91.10(5)	91.40(6)
Cl2–Cu1–Cl3	91.85(5)	92.00(6)
Cl1–Cu1–Cl3	90.65(4)	90.36(7)
Cl3–Cu1–Cl3^{i}	177.17(6)	176.58(7)
Cl1–Cu1–Cl3^{i}	110.04(7)	110.35(9)

Table S3 Site occupancies and equivalent isotropic displacement parameters (Ueq) for Cu and Cl atoms

Atom	x (293 K)	y (293 K)	z (293 K)	Ueq (293 K)	Occ.	x (343 K)	y (343 K)	z (343 K)	Ueq (343 K)	x (368 K)	y (368 K)	z (368 K)	Ueq (368 K)	x (393 K)	y (393 K)	z (393 K)	Ueq (393 K)
Cu1	0.5000	0.37428 (3)	0.17970 (5)	0.0366 (2)	–	0.50000	0.12578 (3)	0.17934 (6)	0.0406 (3)	0.00000	0.12644 (4)	0.17941 (7)	0.0420 (3)	0.50000	0.12744 (5)	0.17997 (8)	0.0487 (5)
Cl1A	0.2774 (19)	0.3137 (7)	0.2625 (12)	0.030 (3)	0.2607 (16)	–	–	–	–	–	–	–	–	–	–	–	–
Cl1B	0.1792 (19)	0.3142 (7)	0.2230 (11)	0.037 (2)	0.2607 (16)	–	–	–	–	–	–	–	–	–	–	–	–
Cl3	0.5000	0.30322 (6)	0.00384 (10)	0.0382 (3)	–	0.50000	0.19688 (6)	0.00368 (12)	0.0446 (4)	0.23355 (3)	0.06424 (7)	0.11638 (15)	0.0709 (5)	0.50000	0.19750 (10)	0.00050 (19)	0.0580 (7)
Cl1	–	–	–	–	–	0.25000	0.18593 (8)	0.25000	0.1182 (15)	0.25000	0.18606 (9)	0.25000	0.0927 (12)	0.25000	0.18677 (10)	0.25000	0.0806 (11)
Cl2	0.26553 (18)	0.43556 (5)	0.11651 (11)	0.0605 (4)	–	0.73411 (2)	0.06430 (5)	0.11615 (13)	0.0642 (4)	0.50000	0.19702 (8)	0.00249 (15)	0.0494 (3)	0.73200 (5)	0.06456 (8)	0.11724 (19)	0.0878 (9)

Table S4 Average equatorial and axial Cu–Cl bond lengths (Å) as a function of temperature

Temperature (K)	⟨Cu–Cl⟩eq (Å)	Cu–Clax (Å)
293	2.263 ± 0.010	2.845(15)
343	2.311 ± 0.056	2.849(19)
368	2.316 ± 0.047	2.861(2)
393	2.304 ± 0.034	2.873(3)

Table S5 Docking results of $(C_5H_9N_3)CuCl_4$ against anti-inflammatory targets.

Target	PDB	Pocket	Vina	Cavity	Affinity	Pathway
iNOS	1NSI	C1	-5.4	6095	Good	NO
5-LOX	3O8Y	C3	-5.2	1950	Moderate	Leukotrienes
COX-2	5KIR	C5	-5.2	2107	Moderate	Prostaglandins
Xanthine Oxidase	1FIQ	C4	-5.1	2198	Moderate	ROS
TNF-alpha	2AZ5	C4	-4.3	244	Weak	Cytokine

Table S6 Molecular docking antimicrobial results showing Vina binding scores, cavity volumes, mechanisms, and estimated MICs for $(C_5H_9N_3)CuCl_4$.

Target	PDB	Vina Score	Cavity (A)	Mechanism
Cu Efflux ATPase	1516	-5.3	546	Pump Inhibition
IscU (Fe-S)	P3W3	-5.0	3569	Metabolism
Catalase	ISJ2	-5.2	11349	ROST

Table S7 Comparison of experimental and theoretical bond lengths (Å) and bond angles (°)

Geometric parameters	Experimental	Theoretical	Δ (%)
Cu1—Cl1	2.273 (2)	2.329	2.4
Cu1—Cl1^{ii}	2.492 (3)	2.527	1.38
Cu1—Cl2	2.253 (2)	2.287	1.24
Cu1—Cl3	2.845 (15)	2.878	1.14
Cl2—Cu1—Cl1	98.18 (7)	99.81	1.63
Cl2—Cu1—Cl1^{ii}	170.90 (6)	173.95	1.75
Cl1—Cu1—Cl1^{ii}	90.74 (5)	93.79	3.25
Cl2—Cu1—Cl3	91.61 (4)	94.67	3.23
Cl1—Cu1—Cl3	96.22 (5)	98.27	2.08
Cl1^{ii}—Cu1—Cl3	85.53 (5)	87.58	2.34
N1—C1	1.317 (6)	1.325	0.60
N2—C1	1.362 (6)	1.368	0.43
N2—C5	1.372 (6)	1.376	0.29
N3—C4	1.459 (6)	1.463	0.27
C4—C5	1.356 (6)	1.360	0.29
C3—C4	1.385 (6)	1.388	0.21
C1—C2	1.385 (6)	1.391	0.43
C2—C3	1.362 (7)	1.370	0.58
C1—N2—C5	121.3 (4)	121.51	0.17
N1—C1—N2	120.3 (4)	120.94	0.53
N1—C1—C2	121.4 (4)	121.49	0.07
N2—C1—C2	118.3 (4)	118.5	0.17
C3—C2—C1	120.6 (4)	120.88	0.23
C2—C3—C4	120.0 (4)	120.15	0.12
C5—C4—C3	119.4 (4)	119.67	0.22
C5—C4—N3	120.6 (4)	120.90	0.25
C3—C4—N3	120.0 (4)	120.12	0.01
C4—C5—N2	120.4 (4)	120.53	0.10

References

1 A. D. Absorption and O. Corrections, *Softw. Correct. Area Detect. Data. Bruker AXS Inc., Madison, WI, USA.*, 2000, 1–8.

2 L. J. Farrugia, *J. Appl. Crystallogr.*, 2012, **45**, 849–854.

3 G. M. Sheldrick, *Acta Crystallogr. Sect. A Found. Crystallogr.*, 2008, **64**, 112–122.

4 G. M. Sheldrick, *Acta Crystallogr. Sect. C Struct. Chem.*, 2015, **71**, 3–8.

5 P. Yadav, C. P. Kaushik, D. Kumar, M. Parshad, A. Yadav and J. Yadav, .

6 P. Yadav, C. P. Kaushik and A. Kumar, *Synth. Commun.*, 2022, **52**, 2149–2162.

7 P. Yadav, C. P. Kaushik, S. Mor, S. Asija, A. Yadav and J. Yadav, *J. Mol. Struct.*, DOI:10.1016/j.molstruc.2025.144704.

8 J. B. Frisch, M.J., Trucks, G.W., Schlegel, H.B., Scuseria, G.E., Robb, M.A., Cheeseman, J.R.; Scalmani, G.; Barone, V.; Petersson, G.A.; Nakatsuji, H.; Li, X.; Caricato, M.; Marenich, A.V.; Bloino, J., Janesko, B.G., Gomperts, R., Mennucci, B., Hratchian, H.P., 2016, https://gaussian.com/gaussian16/.

9 A. D. Becke, *J. Chem. Phys.*, 1996, **104**, 1040–1046.

10 A. V Mitin, DOI:10.1002/jcc.23353.

11 J. M. R. Dennington, T. Keith, *Semichem Inc., Shawnee Mission*, 2009, Semichem Inc., Shawnee Mission:Version 5, https://gaussian.com/citation/.